THE RELATION BETWEEN MICROSTRUCTURE AND CREEP PROPERTIES OF MARTENSITIC 9-12% CR STEELS

H. Cerjak, I. Holzer, P. Mayr, C. Pein, B. Sonderegger and E. Kozeschnik
Institute for Materials Science, Welding and Forming
Graz University of Technology,
Kopernikusgasse 24, 8010 Graz, Austria.

Keywords: 9-12% Cr steels, creep strength, microstructure, microscopy, modelling, simulation

Abstract

In all industrialized countries great efforts are undertaken to lower CO_2 emissions. In the sector of electricity generation progress can be achieved by the improvement of the efficiency of fossil, especially coal fired, power plants. Efficiency improvements can be obtained by increasing the steam parameters, temperature and pressure. For components exposed to critical steam cycle loads the availability of improved high temperature creep resistant materials, including their weldments, is required. Research activities on ferritic/martensitic 9-12% Cr steels at Graz University of Technology are represented by a network of interacting projects focusing on mechanical properties of base and weld metal, damage kinetics, weldability, microstructure analysis in the course of creep, modelling of precipitation and coarsening kinetics, simulation of complex heat treatments and the deformation behaviour under creep loading. The individual projects are briefly described and the conceptual approach towards a quantitative description of the creep behaviour of 9-12% Cr steels is outlined.

Introduction

For many components in thermal power plants, creep resistant martensitic-ferritic 9-12% Cr steels are used because of their good creep resistance, oxidation behavior and low thermal expansion coefficient. The main challenge in the development of these steels are the increase of the creep resistance at temperatures greater than 600°C, for both, base material and weldments. Final goal is to reach a creep resistance for loads of 100MPa and exposing times of more than 10^5h. In the past, often short time creep tests were used in order to extrapolate the lifetime of the components. Although many steels show optimal microstructure after the heat treatment, but show a drop in the creep resistance after about 10^4h. Mainly, two reasons are responsible for this deterioration: First, creep mechanisms change when applying different creep loads. Usually, these mechanism changes are not considered when extrapolating lifetimes of components. Second, the microstructure of the material undergoes an evolution: precipitates coarsen and dissolve, other precipitates form, martensite laths broaden etc.

This change in microstructure is not incorporated into macroscopic extrapolation methods. Both aspects are considered in the comprehensive approach, which is presented in the following.

Metallographic investigations

Several microscopical techniques combined in order to overlap their information content. Following microstructural features were examined: Size of martensite laths and subgrains; the size distribution, number density, type and location of precipitates and the size and location of pores.

Many works on these topics have been published so far: Hättestrand and Andren [1-4], Hofer et al. [5-9], Hofer and Cerjak [10-13], Strang and Vodarek [14, 15], Kimura et al. [16], Papst [17-19], Danielsen and Hald [20] and Sonderegger [21, 22] measured size and chemical composition of precipitates via TEM/EFTEM or atom probe. Korcakova, Hald and Somers [23] and Dimmler [24-26] investigated Laves-phase precipitates by SEM. Investigations of size and distribution of creep pores were also carried out by Dimmler. Martensite lath width and size of subgrains were measured by Sklenicka [27], Cerri [28], Sawada [29, 30], Sonderegger [21, 31] and others. However, the isolated investigation of different features is not sufficient, only the combination of techniques and the implementation of the results into numerical simulation tools will enhance the knowledge and understanding sufficiently.

Sub-µm precipitates: TEM/EFTEM

The following work mainly concentrates on the creep resistant 9-12% Cr COST steel variant CB8. The chemical composition is given in Tab. 1.

Table 1: Chemical composition of the steel CB8 (wt%).

Al	B (ppm)	C	Co	Cr	Mn	Mo	N	Nb	Ni	Si	V
0.028	0.0112	0.17	2.92	10.72	0.20	1.40	0.0319	0.06	0.16	0.27	0.21

Transmission-electronmicroscopy (TEM) and energy-filtered TEM (EFTEM) are ideal methods to measure size, shape and number density of small (<1µm) precipitates. In order to determine the chemical composition, EELS (Electron Energy Loss Spectroscopy) and EDX is applied. Additional methods like CBED (Convergent Beam Electron Diffraction) or SAD (Selected Area Diffraction) are necessary to get informations on the crystal structure of the precipitates.

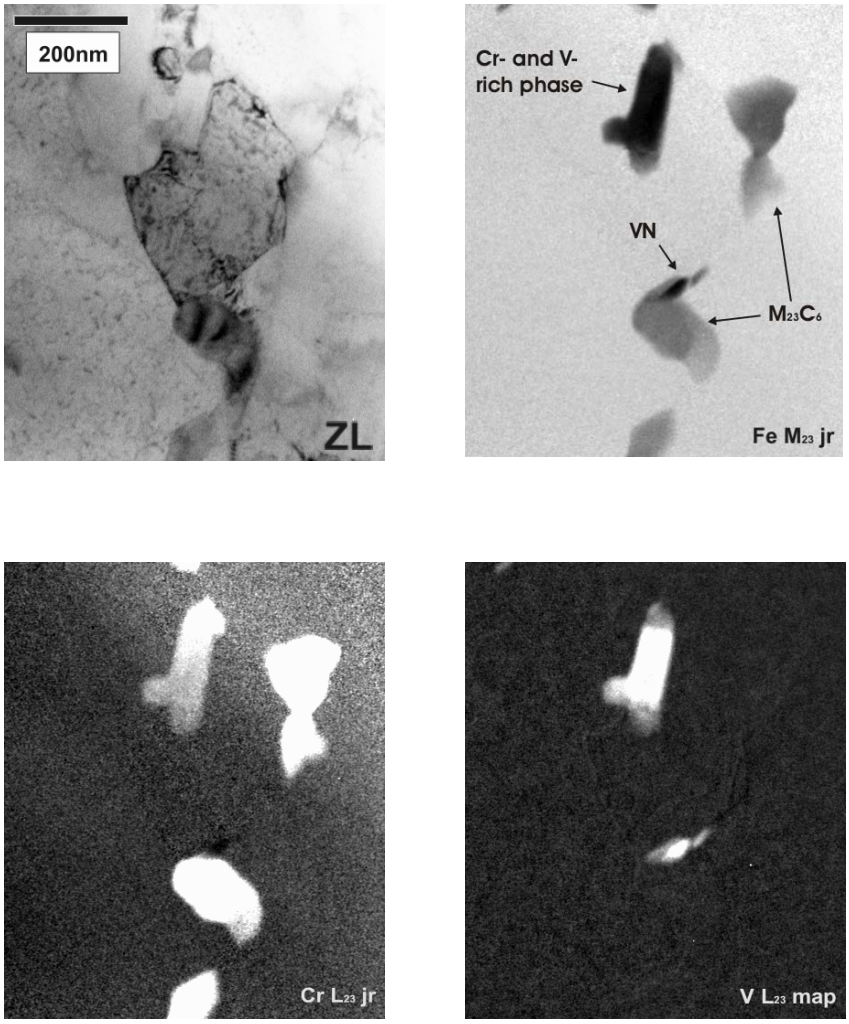

Figure 1: Cr-carbides ($M_{23}C_6$), V-nitrides (VN) and a Cr and V-rich phase, measured by EFTEM jump ratio images and elemental maps

Figure 1 shows EFTEM micrographs of different precipitate types in a thermally aged sample of the creep resistant 9-12% Cr steel CB8. The combination of EFTEM micrographs (indicating the local composition) with zero loss images (indicating matrix boundaries, dislocations etc.) gives valuable information on the local microstructure near the precipitates. Additionally, the size and number density can be measured as a function of creep loading and tempering time [3, 22, 32]. Figure 2 shows the results on thermally aged samples of the material CB8:

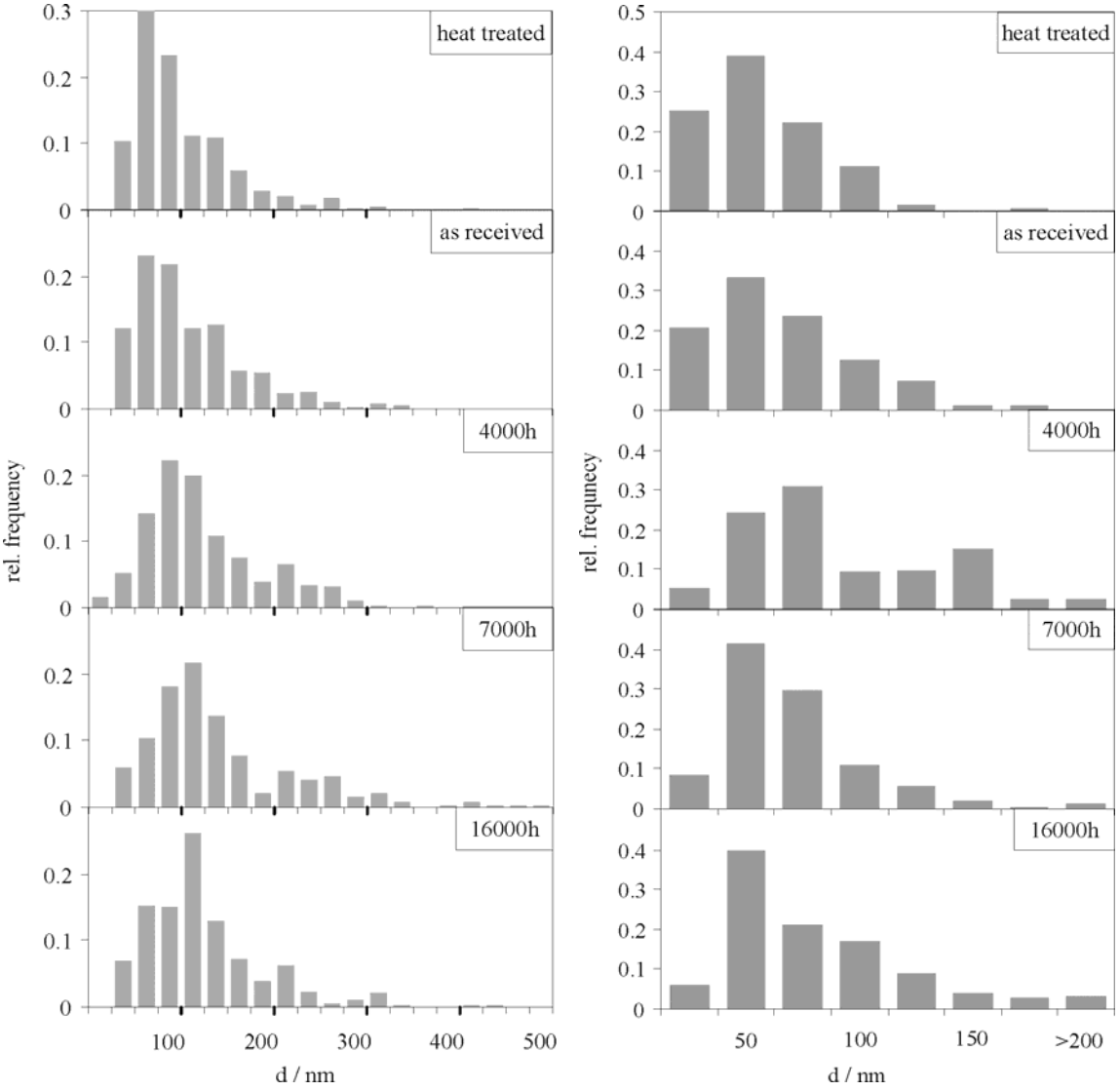

Figure 2: Size distributions of $M_{23}C_6$ precipitates (left diagram) and VN (right) after one heat treatment cycle (heat treated), as received condition, and several durations (4000h, 7000h, 16000h) of overageing at 650°C

Precipitates greater than 0.5-1µm

For precipitates greater than 0.5-1µm, Scanning Electron Microscopy (SEM) is much more convenient. Particles of this size usually provide lower number densities, which are unsuitable for investigations in TEM. According to Reuter [33], precipitates can be visualized due to their Z-contrast relative to the matrix, thus the chemistry must be sufficiently different. Table 2 shows calculated contrasts of several precipitate types relative to the matrix of a 9-12% Cr steel. Laves phase has the best combination of great diameters and good Z-contrast due to its high Mo- or W- content.

Table 2: Chemical composition, calculated Z-contrast and mean diameters of several precipitate types in 9-12% Cr steels [34]

Precipitate type	Z-contrast	d [nm]
$M_{23}C_6$	-2%	50-200
VN	-5%	10-100
Nb(C,N)	16%	10-100
Laves phase	28%	200-2000
Z phase	-4%	50- 1000

Creep voids

View damage investigations can be found in literature [35], but in order to understand the creep behavior in the tertiary regime, also the evolution of creep pores have to be considered. Figure 3 shows the spatial distribution of creep pores in the vicinity of the fracture surface of a broken creep sample. Following steps are necessary for the metallographic investigations:

- Special preparation techniques for even very small creep pores [25]
- Automatic image processing and evaluation
- Reconstruction of position oft he pores relative to other microstructural components, such as precipitates or grain boundaries

These systematic evaluations lead to an improved understanding for the formation of creep pores up to macroscopic damage of the material in the tertiary creep regime.

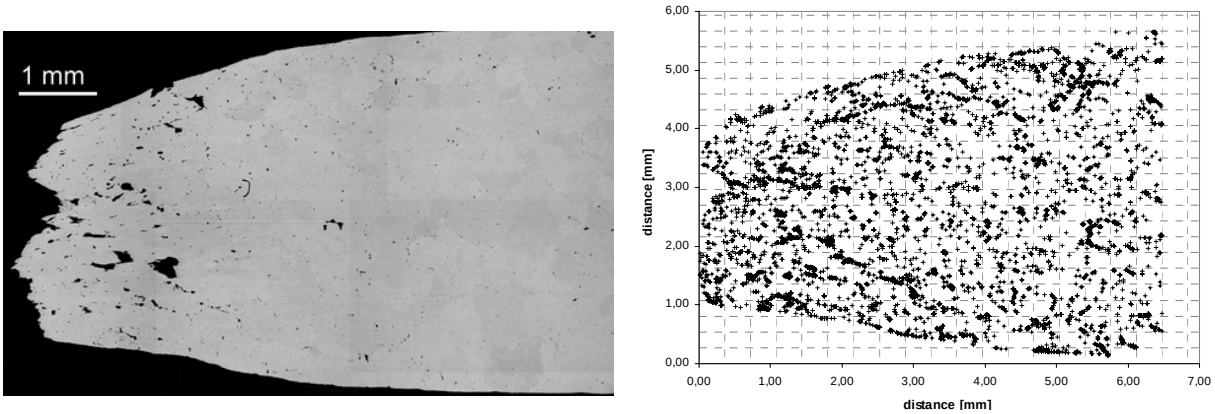

Figure 3: SEM micrograph of a broken creep sample (CB8, left image) plus reconstruction of the position of creep pores (right image)

Martensite laths and grains: EBSD

By EBSD (Electron Backscatter Diffraction) in SEM, grains, subgrains and martensite laths can be differed via measuring crystal orientations. The spatial resolution reaches down to approximately 200nm and an orientational resolution of 1-1,5°. Not only the size and shape of grains can be measured – also informations regarding the matrix boundary are available, like misorientation or deviation from an ideal twin boundary. This, EBSD also provides indirect information on boundary energy or mobility. Figure 4 shows an EBSD map of steel CB8; single martensite laths are shown by different brightness. Figure 5 shows the evaluation of a number of thermally aged or creep loaded samples regarding the subgrain size. It is clearly visible, that thermally ageing (at 650°C) alone does not produce a significant amount of subgrain coarsening, whereas additional creep loading (80-110MPa) does.

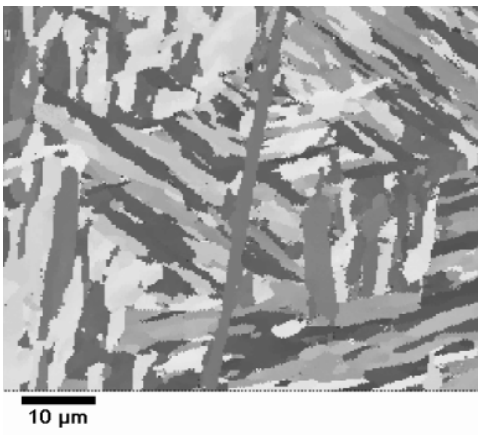

Figure 4: EBSD micrograph of CB8, thermally aged

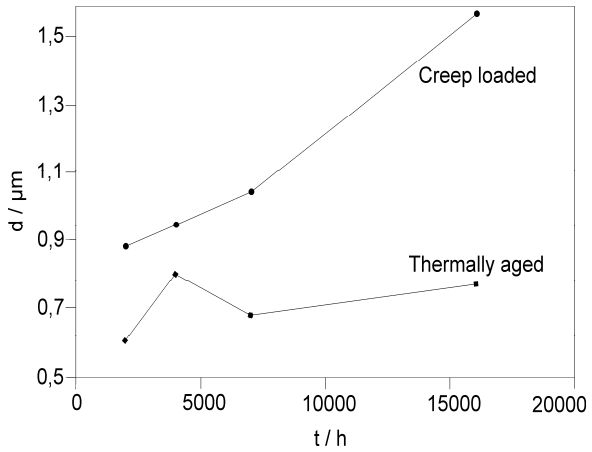

Figure 5: Mean Subgrain diameters of thermally aged or creep loaded samples

Weldability assessment

For a successful service application and acceptance in practice, the weldability and the long-term behaviour of welds of the newly developed materials is one of the key issues. Therefore, the weldability of several 9-12%Cr steels is investigated at the IWS. Microstructural evolution during welding is studied by heat affected zone (HAZ) simulation using a Gleeble thermo-mechanical simulator and subsequent metallographic investigations applying most advanced electron microscopic methods. The creep strength of base materials, weld metals and cross-welds is studied by long-term creep testing at service temperature.

Creep strength of cross-welds is decreasing with increasing testing duration compared to the mean base material creep strength. This decrease in creep strength is independent of the selected weld metal. Figure 6 shows results of creep tests at 600°C of cross-welds fabricated with three different filler metals differing in weld metal creep strength. After 10.000 hours of testing cross-weld creep strength deviates from the mean line of base material creep strength. After 30.000 hours of testing, creep rupture strength of cross-welds is already approximately 30% below the base material creep

strength independently of the weld filler. The mismatch in creep rupture strength between base material and cross-welds is expected to increase further with increasing testing duration.

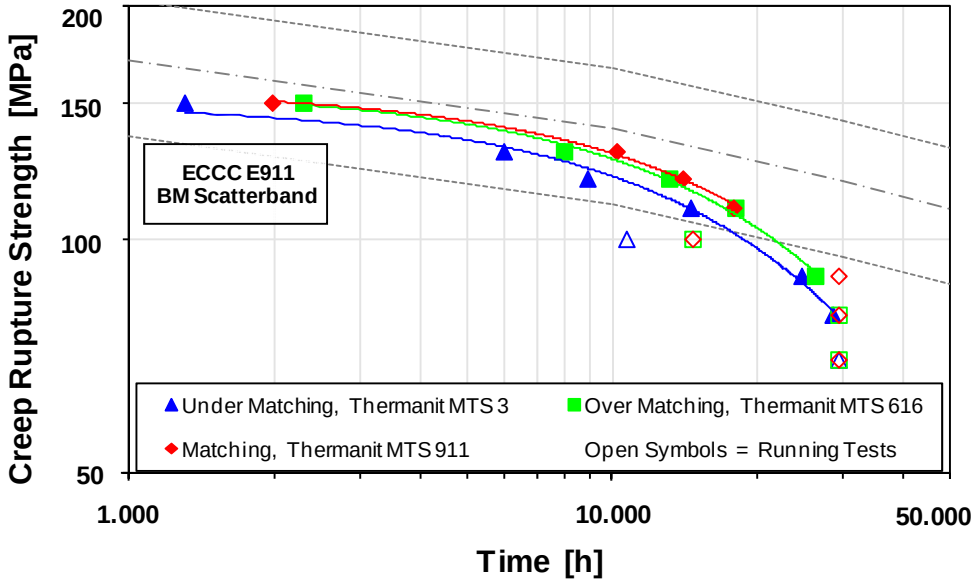

Figure 6: Creep rupture data at 600°C for welds of G-X11CrMoWVNb 9-1-1 (E911). Comparison of the cross-weld creep strength to the mean creep strength of E911 base material.

Type IV cracking in the fine-grained HAZ has been identified as major reason for the decrease of cross-weld creep strength. In Figure 7, the fracture location investigation of a creep tested cross-weld of G-X11CrMoWVNb 9-1-1 (E911) parent cast material welded with a strength matching filler material is shown. Failure takes place in the fully refined region of the HAZ (see Figure 8). Creep damage by formation of voids is limited to a very narrow region parallel to the weld fusion line adjacent to the unaffected base material.

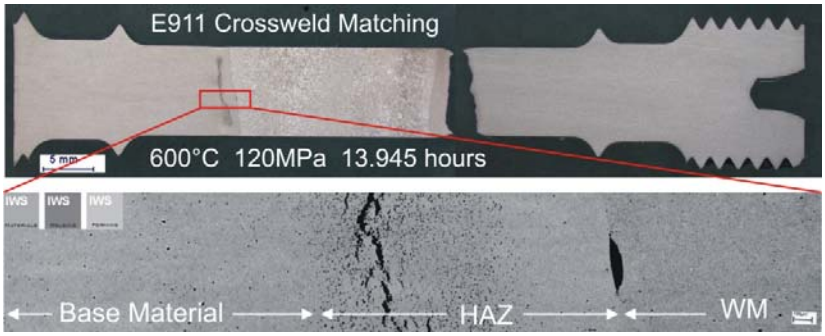

Figure 7: Fracture location investigation of a creep tested cross-weld sample. E911 pipe material welded with Thermanit MTS 911 (matching creep strength level). Excessive pore formation in a 1 mm wide zone adjacent to the unaffected base material.

Creep at low stress levels as a diffusional problem is enhanced in a microstructure containing a high volume fraction of prior austenite grain boundaries. All diffusion driven processes, e.g. recovery or coarsening of precipitates are proceeding much faster in this region of the HAZ compared to the weld metal, unaffected base material or other HAZ regions.

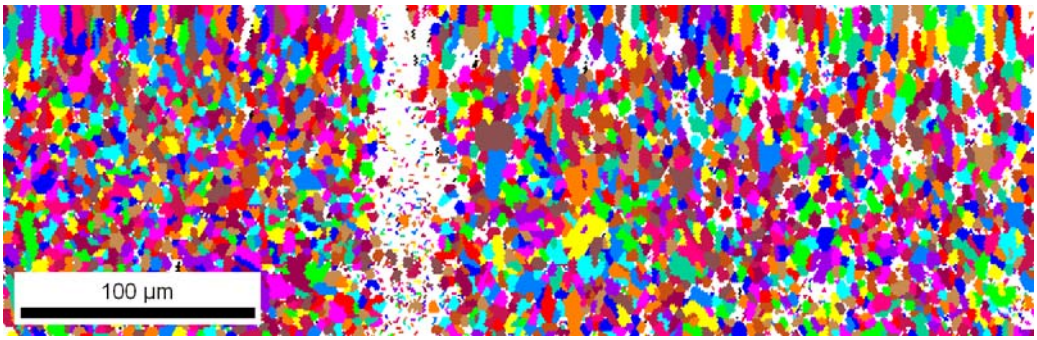

Figure 8: EBSD grain mapping at the location of fracture in specimen shown in Figure 7. Crack and creep voids are represented by white areas within the image.

Figure 9 shows a comparison of the initial microstructure in the grain-refined region of a cross-weld after post-weld heat treatment and the same region after 14.000 hours of creep exposure at 600°C. The number density of precipitates decreases during creep and the average diameter of the precipitates increases. Both results in a decrease of creep strength in this part of the HAZ.

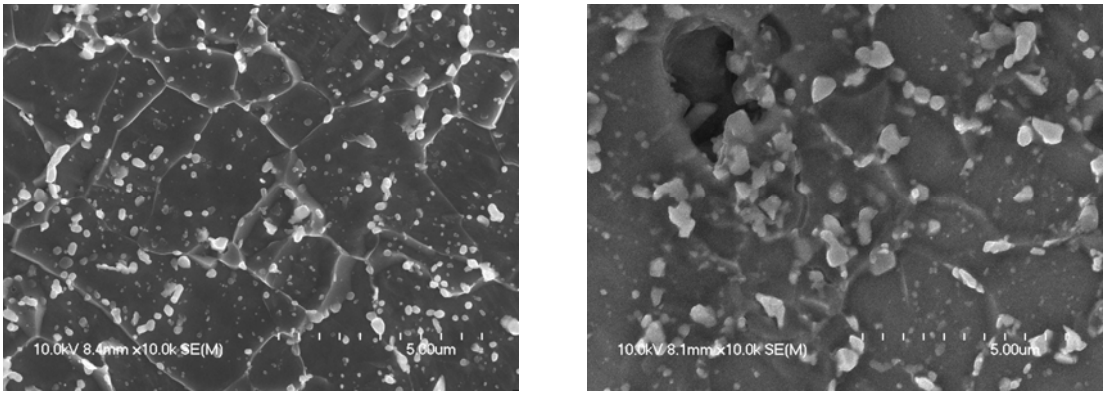

Figure 9: Microstructural evolution during creep in the fine-grained HAZ of E911 cross-welds tested at 600°C. Precipitates of the initial microstructure (left) show extensive coarsening during 14.000 hours of creep exposure.

Type IV cracking has been identified as the major end-of-life failure mechanism in creep exposed welded structures of 9-12% Cr steels. So far, the reduced cross-weld creep strength can only be considered by the introduction of a weld strength factor during the design of components. Further research at the IWS heads into the direction of the suppression of a fully refined microstructure in the HAZ by modifications of base material chemistry with controlled addition of boron and nitrogen. This allows increasing the creep strength of cross-welds to the level of the base material and eliminating Type IV cracking

Thermodynamic and kinetic simulations

In the last years thermodynamic and kinetic simulations have become increasingly important when optimizing the chemical composition and production process [36]. Since the long-term stability of the microstructure of 9-12% Cr-steels is closely related to the stability of the precipitate microstructure, it is very important to describe and predict the evolution of each precipitate population during the entire lifetime of a component. Based on a recently developed theoretical approach for the simulation of the precipitation kinetics of multi-component multi-phase materials [37, 38], the evolution of the precipitate microstructure during heat treatment and service of the COST steel CB8 has been simulated on the computer.

Thermodynamic equilibrium analysis

The thermodynamic equilibrium analysis is an important step in a comprehensive material characterization. Figure 10 shows the calculated phase diagram for the steel CB8 as a function of carbon content. For the calculation a slightly modified version of the thermodynamic database TCFE3 was used, e.g. to account for the stabilizing effect of silicon on the Laves phase [24]. Moreover, although not considered in the phase diagram below, a revised thermodynamic description for the modified Z-phase [42] has been added to this database, which is a further development of the initial assessment of Danielsson and Hald [20]. These values have been used in the kinetic simulations presented in the following section.

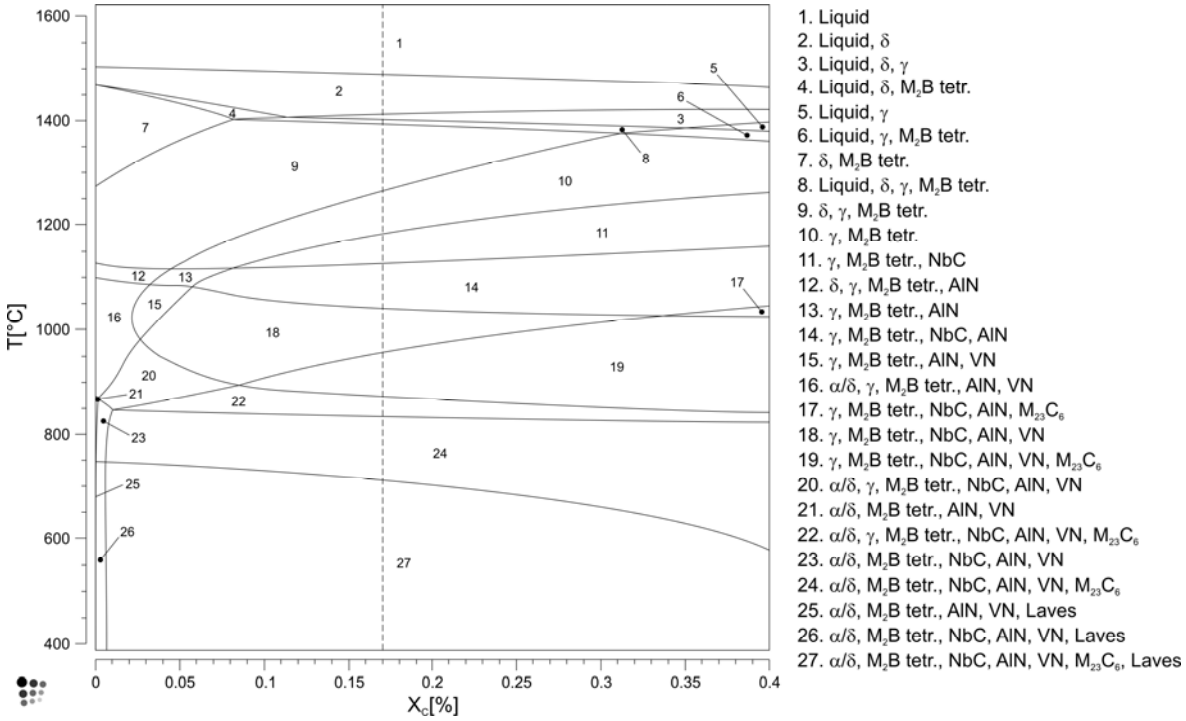

Figure 10: Calculated phase diagram of the COST alloy CB8.
A modified version of the TCFE3 database was used.

Kinetic simulation

Beside thermodynamic equilibrium calculations also kinetic simulations have to be carried out to reach a better understanding of the effect of precipitate evolution. Therefore the industrial heat treatment for the COST alloy CB8 was simulated with the kinetic simulation software MatCalc [41]. The underlying theory and model implementation is described in refs. [37- 40]. For the simulation a modified version of the database TCFE3 and the diffusion database Mobility_v21 from ThermoCalc AB, Stockholm, Sweden were used. The adaptions were made based on the experimental observations in [21]. The simulation result for the heat treartment is shown in Figure 11.

The top figure shows the temperature history during heat treatment. The simulation starts closely below the solidus temperature of this material, i.e. 1400 °C. Cooling proceeds down to 350°C. At this temperature, the austenite matrix decomposes into martensite. It is assumed that no precipitation reactions occur below this temperature due to the sluggish diffusion. In the next simulation step, the temperature is increased again. The simulation is performed in a ferritic matrix up to 847°C, the A_1 temperature of this steel. Then, the matrix is changed to austenite again and austenitization takes place at 1080 °C. The three quality heat treatment cycles take place again in a ferritic matrix. The two lower graphs show the results of the simulation of the time temperature sequence explained above. The phase fraction of the $M_{23}C_6$ and Laves phase is divided by a factor of ten to get a more concise diagram. These results are compared to experimental data measured by one of the authors [21]. Good agreement is observed between simulation and experiment. A more detailed description of the heat treatment simulation is given in [43].

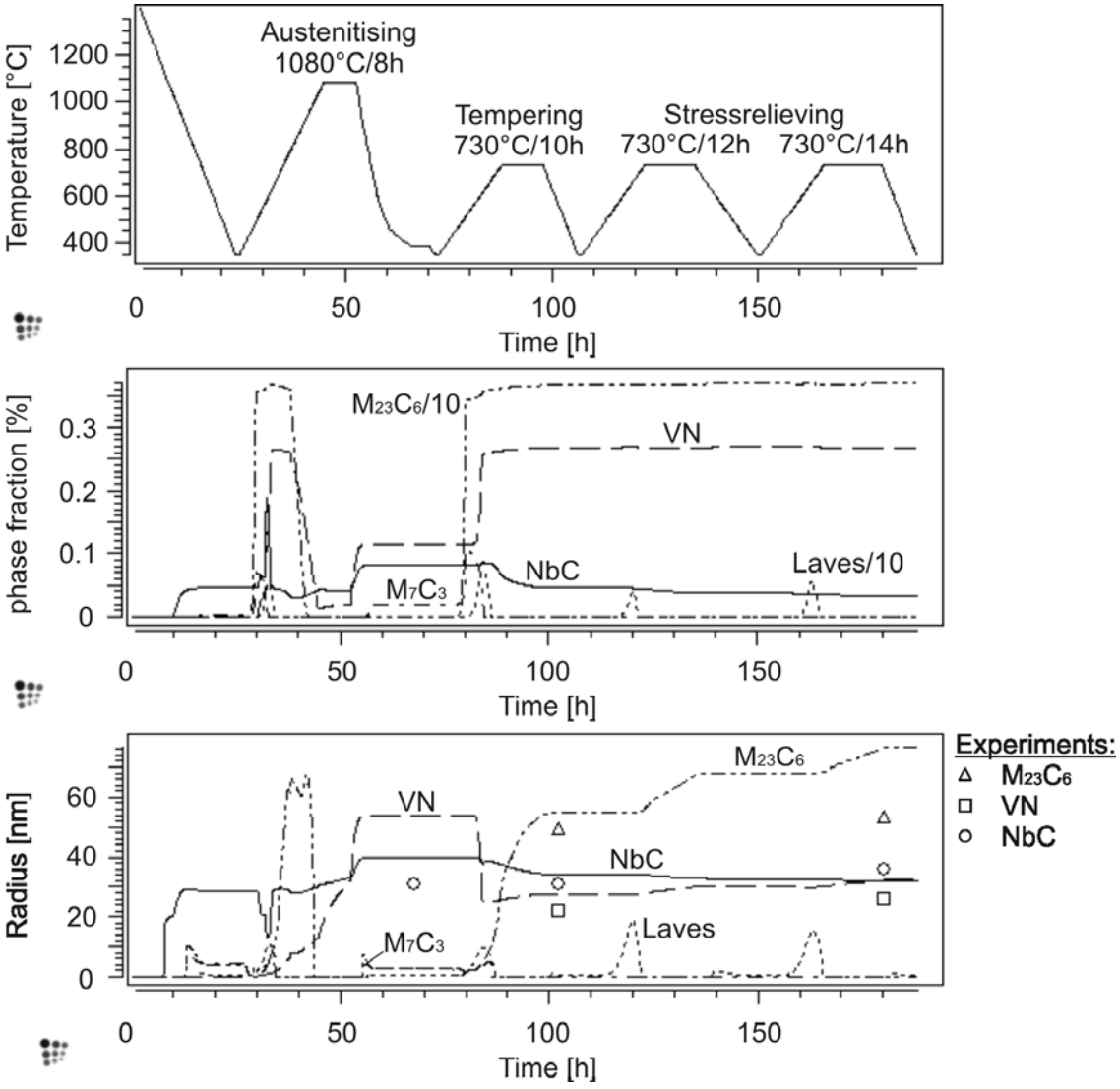

Figure 11: Results of the heat treatment simulation of COST alloy CB8

Microstructure modelling

In oreder to predict the behavior of creep resistant steels, the full complexity of the creep process can only be described with models that can cover all physical mechanism that interact in the material. A comprehensive microstructural model of creep must include, for instance, diffusional creep, dislocation dynamics as well as all interactions between the microstructural components, such as dislocations, grain boundaries and precipitates. It was also proposed that local effects must be taken into account, because any weak spot in the microstructure can cause ultimate failure of the macroscopic component [45]. Therefore, to give a short overview about the ongoing modelling activities, two different approaches are outlined in the following which are developed or applied at the IWS: the back-stress concept and a newly developed spatially resolved model for the evolution of the local microstructure.

Back-stress concept

If an external force is acting on a microstructure, it is frequently assumed that the external load σ_{ex} is counteracted by heterogeneous internal microstructural constituents, such as precipitates and interfaces. Consequently, not the entire external load can be assumed to represent the driving force for the creep process; only this part of the external stress σ_{ex}, which exceeds the amount of inner stress σ_i from the counteracting microstructure, effectively contributes to the creep process. Since the inner stress reduces the effect of the external stress, this approach is commonly denoted as back-stress concept. The effective creep stress σ_{eff} can be expressed as

$$\sigma_{eff} = \sigma_{ex} - \sigma_i . \quad (1)$$

In a recent treatment by Dimmler [24], the inner stress σ_i has been expressed as a superposition of individual contributions from dislocations and precipitates. When also taking into account the contribution from subgrain boundaries, the inner stress is

$$\sigma_i = M\tau_i = M(\tau_{disl} + \tau_{prec} + \tau_{sgb}) , \quad (2)$$

where M is the Taylor factor (usually between 2 and 3, see ref. [24]) and τ is the shear stress. The subscripts in the bracket term denote contributions from dislocations, precipitates and subgrain boundaries, respectively. The concept of the effective and inner stress to describe the creep behavior is shown in Figure 12. The input parameters are the applied stress σ, temperature T and time t [24].

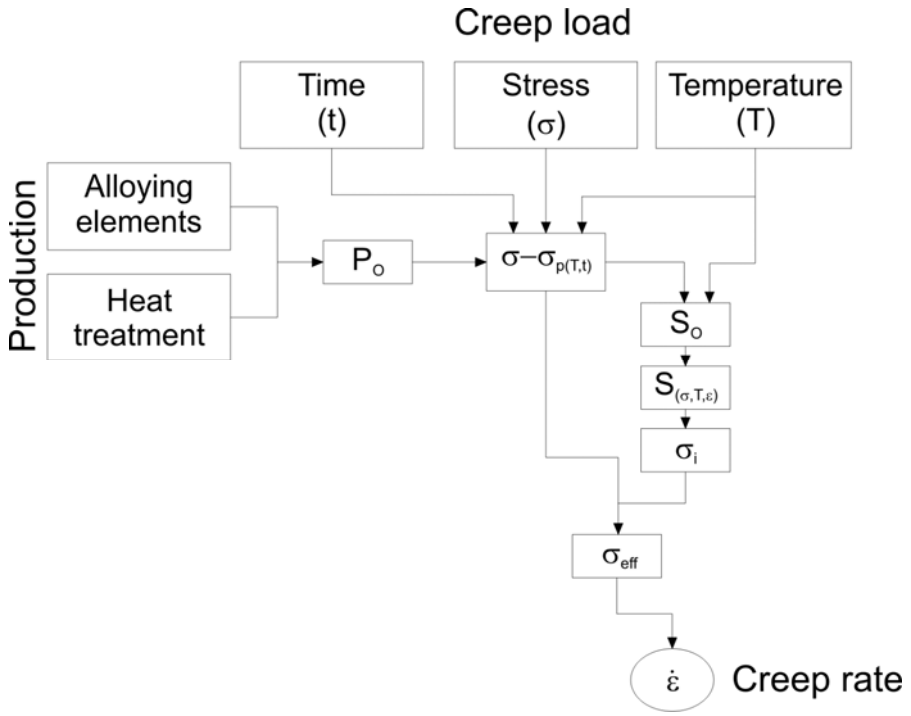

Figure 12: Back-Stress concept, scematic [47]

The combination of the back-stress concept with the simulation software MatCalc allows therefore determining at every point the inner stress, which influences the plastic deformation, as a function of

the microstructural evolution. First results and more detailed information about the theoretical approach are given in an accompanying paper [46].

Microstructure simulation

If an external stress is applied on a poly-crystalline, multi-phase microstructure, the resulting microscopic stress field within the specimen will usually show a complex pattern of areas with alternating compressive and tensile stresses. This pattern strongly depends on the local microstructure and its elements as precipitates, pores, grainboundaries etc. For this reason phenomenological and statistical approaches cannot capture the essential microstructural changes that occur in the material on a local scale. In our model these local phenomena shall be considered, including self-diffusion of vacancies, motion of dislocations, kinetics of precipitation and other effects, as well as interactions among them.

In our opinion, phenomenological and statistical approaches cannot capture the essential microstructural changes that occur in the material on a local scale. Important physical processes in creep, such as nucleation and growth of micro-voids or dissolution of precipitates, operate on a local basis, and, therefore, an appropriate model must take these local events into account. Only by these means modelling and simulation can support our conception of creep.

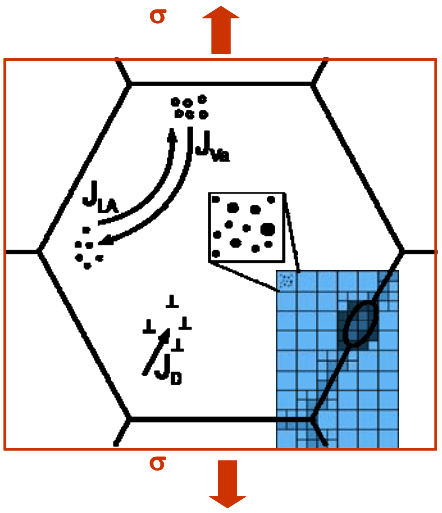

Figure 13: Microstructural model

Figure 13 presents a sketch of our local microstructure approach illustrating the basic mechanisms and interactions. The flux of vacancies which is caused by local microscopic stresses produces mass transport in the opposite direction. Motion of dislocation is activated by the local stress gradient. Moving boundaries interact with precitpitates within the matrix and vice versa. Depending on these mechanisms creep can be divided into diffusional creep, creep caused by dislocations and other effects. The model development now is focused on the correct specification of diffusional creep, which is the predominant process at low stresses [48].

There are two main mechanisms which are causing diffusional creep, namely diffusion via the bulk and diffusion via grain boundaries.

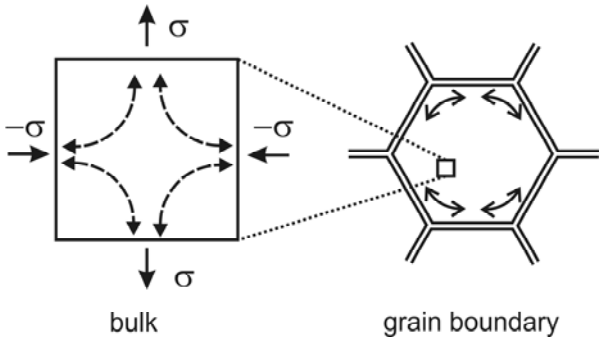

Figure 14: Finite element model for the simulation of diffusional creep

Two boundary conditions are relevant for the description of the flux in the matrix: The characterisation of the flux itself (Ficks Law) and the calculation of the concentration of vacancies in equilibrium, dependent of the local stress distribution. The output of the calculations is the spatially distributed flux of vacancies and the resulting time dependent deformation of the material.

The behaviour of grain boundaries differs from that of the grain itself. The main reason is the different reaction on shear stress – two grains glide along the grain boundary when shear stress is applied. This behaviour is modelled with a stong anisotropic tensor of the Elastic Modulus.

In our simulation, the microstructure is discretized with rectangular cells, each of them corresponding to a representative volume of the simulation domain. Each element can be one single phase, e.g. matrix, carbide or a grain boundary and, accordingly, material properties such as Young's modulus, shear modulus etc. are assigned to it.

As a first example for our microstructure model, we consider a hard lens-shaped precipitate within a homogeneous soft matrix. An external stress in the y axis is applied, which causes a local stress distributiuon and deformation. Figure 15 shows first results of our simulation.

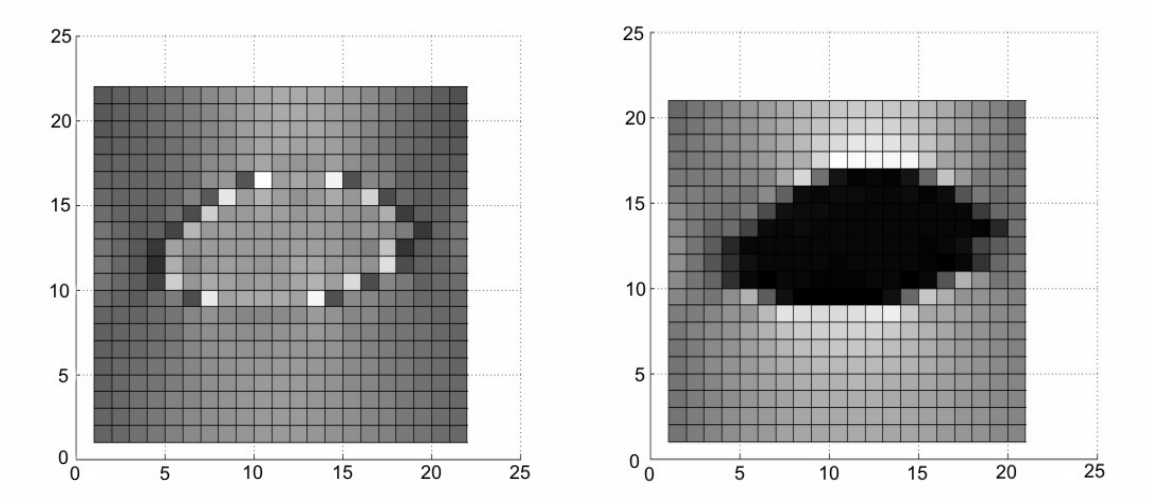

Figure 15: Elastic stress field near a hard precipitate.
Von Mises stress (left) and elastic deformation (right)

Conclusion and Outlook

Material development of creep resistant 9-12% Cr steels in thermal power plants has become increasingly complex. Many steel variants show superior creep resistance within the first year of service, but a pronounced drop at longer exposure times. In order to overcome this degradation, it is necessary to investigate the material by different methods with overlapping information content, understand the evolution processes, and simulate the microstructural evolution. Models, which have been used in the past, like estimating the lifetime by short term creep experiments, show the danger of being too optimistic regarding the estimated lifetime of the components. The comprehensive approach presented in this paper overcomes these difficulties and shows the potential of reducing development costs and time.

References

1 M. Hättestrand, H. O. Andrén, Materials Science and Engineering. A270 (1999), 33-37.

2 M. Hättestrand, M. Schwind, H. O. Andrén, Materials Science and Engineering. A250 (1998), 27- 36.

3 M. Hättestrand, H. O. Andrén, Micron 32 (2001), 789- 797.

4 M. Hättestrand, H. O. Andrén, Acta mater. 49 (2001), 2123- 2128.

5 F. Hofer, P. Warbichler: Ultramicroscopy, 63 (1), 1996, 21-25.

6 F. Hofer et al., J. Microscopy, 204 (2), (2001), 166.

7 P. Warbichler, F. Hofer, P. Hofer, E. Letofsky, H. Cerjak, Micron (1998), 63-72

8 F. Hofer, P. Warbichler, B. Buchmayer, S. Kleber, Journal of Microscopy 184 (1996), 163-174

9 F. Hofer et al., Metallurgical and materials transactions A 31A (2000), 975

10 P. Hofer. PhD thesis, Technische Universität Graz, 1999.

11 P. Hofer, H. Cerjak, B. Schaffernak, Steel research 69 (1998) 8, 343-348

12 P. Hofer, H. Cerjak, P. Warbichler, Materials Science and Technology 16 (2000), 1221-1225

13 H. Cerjak, P. Hofer, B. Schaffernak, P. Warbichler, Praktische Metallographie 27 (1997)

14 A. Strang, V. Vodarek, Proc. Microstructural development and Stability in high Chromium ferritic power plant steels, Cambridge, 1995, 31-51.

15 V. Vodarek, A. Strang, Materials for advanced power engineering, Liege, 2002, 1223-1231.

16 K. Kimura et al., Proc. Materials for advanced power engineering, Liege, 2002, 1171-1180.

17 I. Papst et al., Metallographietagung Dortmund, Germany, 6.-10. September 1999

18 I. Letofsky-Papst et al., Zeitschrift für Metallkunde 95 (2004) 1, 18-21

19 I. Letofsky-Papst et al., Praktische Metallographie 41 (2004) 7, 334-343

20 H. Danielsen, J. Hald, ISSN 0282-3772, Värmeforsk Service AB, Stockholm, 2004

21 B. Sonderegger, PhD thesis, Technische Universität Graz, 2005

22 B. Sonderegger, Ultramicroscopy 106 (2006) 10, 941-950

23 L. Korcakova, J. Hald, M. Somers, Materials Characterisation 47 (2001), 111- 117.

24 G. Dimmler, PhD thesis, Technische Universität Graz, 2003

25 G. Dimmler et al., Praktische Metallographie, 39 (2002) 12, 619-633

26 G. Dimmler et al., Materials Characterization 51 (2003), 341-352

27 V. Sklenicka, K. Kucharova, A. Dlouhy, J. Krejci, Proc. Materials for Advanced Power Engineering 1994. Liége (1994), 435- 444.

28 E. Cerri, E. Evangelista, S. Spigarelli, P. Bianchi, Materials Science and Engineering. A245 (1998), 285-292.

29 K. Sawada. et al., Materials Science and Engineering. A267 (1999), 19- 25.

30 K. Sawada, K. Kubo, F. Abe, Materials Science and Engineering. A319- 321 (2001), 784- 787.

31 B. Sonderegger, S. Mitsche, H. Cerjak, Materials Characterization, in print

32 E. E. Underwood: Quantitative Stereology, London, 1970, 174

33 W. Reuter. In: Shinoda G, Kohra K, Ichinokawa T, editors. Proceedings of the 6th International Congress on X-ray Optics and Microanalysis. Tokyo: University of Tokyo Press (1972), 121.

34 P. Weinert et al., proc. MPA Seminar (2002)

35 W. Poeppel, U. Hildebrandt, Praktische Metallographie; 26 (1989); 141-153.

36 J. O. Andersson, T. Helander, L. H. Höglund, P. F. Shi, B. Sundman, CALPHAD, vol. 26, Nr. 2 (2002), 273-312

37 J. Svoboda, F. D. Fischer, P. Fratzl, E. Kozeschnik, Mater. Sci. Eng. A, vol. 385, Nrs. 1-2, (2004), 166-174

38 E. Kozeschnik, J. Svoboda, F. D. Fischer, CALPHAD, vol. 28, Nr. 4, (2005), 379-382

39 J. Svoboda, I. Turek, F. D. Fischer, Phil. Mag., vol. 85 (2005), 3699-3707

40 L. Onsager, Physical Review, I. vol. 37, pp. 405-426, (1931), II. vol. 38 (1931), 2265-2279

41 Software package, MatCalc, http://matcalc.tugraz.at.

42 H. Danielsen, private communication

43 E. Kozeschnik, B. Sonderegger, I. Holzer, J. Rajek, H. Cerjak; Materials Science Forum Vols. 539-543 (2007), pp. 2431-2436

44 J. Rajek, PhD thesis, Graz University of Technology, 2005.

45 P. Weinert: Microstructural Modelling of Creep in Ferritic/Martensitic 9-12% Cr-Steels, PhD thesis, Graz University of Technology, 2001.

46 I. Holzer, E. Kozeschnik, H. Cerjak, this issue

47 B. Reppich: Zeitschrift für Metallkunde, 73 (11), (1982), 697-805

48 F.R.N. Nabarro, Met. Mater. Trans., Vol 33A, (2002), 213-218.